***Adam K. Puszkarz,
Izabella Krucińska**

Lodz University of Technology
Faculty of Material Technologies
and Textile Design
Department of Material and Commodity Sciences
and Textile Metrology
Zeromskiego 116, 90-924 Lodz, Poland
* E-mail: adam.puszkarz@p.lodz.pl

Study of Multilayer Clothing Thermal Insulation Using Thermography and the Finite Volume Method

Abstract
The article concerns the wide issue which is thermal comfort. In the paper investigations on the textile thermal insulation problem are presented. Materials tested were multi-layer systems with potential application in uniforms addressed to firefighters. Thermal insulation was tested both experimentally (using a thermal imaging camera) and by modelling (by means of simulations of heat transfer phenomena on 3-D models of real textiles). The materials investigated were constructed with the following raw materials: Kevlar, Nomex, ePTFE, PU and carbon fiber. Textiles with a comparable geometric structure and similar composition were tested for their thermal insulation. In the experimental part temperature, the change in specific constant ambient conditions was obtained using a thermal imaging camera. In the simulation part 3-D models of actual textiles were designed and the temperature change was calculated on the basis simulations of the real experiment performed . For each multi-layer system two models were designed, with varying degree of mapping the structure of the yarn in the fabrics. The main goal of the work was experimental verification of both models. As a result of the simulation performed on a model characterised by a more accurate mapping of the yarn structure, comparable results were obtained with experimental data and a strong relationship of thermal insulation textiles from the composition of raw materials and the geometric structure was confirmed.

Key words: *fabric, simulation, heat transport phenomena, thermal insulation, modelling, thermography, finite volume method.*

Nomenclature

e *specific internal energy, J*

h *thermal enthalpy per unit mass, $J \cdot kg^{-1}$*

p *pressure, Pa*

Pr *Prandtl number, dimensionless*

Q_H *heat change (released or absorbed) per unit volume, $W \cdot m^{-3}$*

Q_T^{out} *heat radiation leaving a radiative surface, $W \cdot m^{-2}$*

Q_T^{in} *incident thermal radiation arriving at surface, $W \cdot m^{-2}$*

q_i *diffusive heat flux density, $W \cdot m^{-2}$*

T *temperature, °C*

u *fluid velocity, $m \cdot s^{-1}$*

ε *surface emissivity coefficient of thermal radiation, dimensionless*

λ_i *eigen values of thermal conductivity tensor, $W \cdot m^{-1} \cdot °C^{-1}$*

λ *thermal conductivity, $W \cdot m^{-1} \cdot °C^{-1}$*

μ *dynamic viscosity coefficient, $Pa \cdot s$*

μ_t *turbulent eddy viscosity coefficient, $Pa \cdot s$*

ρ *fluid density, $kg \cdot m^{-3}$*

σ *Stefan Boltzmann constant, JK^{-1}*

τ_{ik} *viscous shear stress tensor, Pa*

■ Introduction

The feeling of thermal comfort is the result of many factor related to the human body, for example climatic conditions of the environment and clothing, which is a barrier that protects the body against the negative influence of external factors. The impact of clothing i.e. the process of heat exchange between the human body and the environment depends largely on the structure of the material, ie. the number and configuration of the individual layers of clothing, as well as on the properties of thermal insulation of materials from which the clothing complex is made. Thermal features are the basic ones that should be considered in relation to the potential user of clothing. Thus the heat exchange between the user and the environment should be balanced to ensure comfortable conditions and prevent both hypothermia and hyperthermia.

The structural modelling of textiles is a tool promoting better understanding of the impact of morphology on their physical properties. In addition, it could provide information on the critical parameters of materials that make up a particular type of fabric, influencing significantly selected physical properties of the product designed. Thermal properties are basic characteristics to consider with respect to the potential user of clothing.

Over the last few years, designing textile models to better understand the impact of morphology on thermal and mechanical properties has been the subject of many studies. With increasing computing power the accurate models produced better address the construction of actual materials and their physical properties.

Qiong-Gong Ning et al. [1] presented a micromechanics model developed to predict the in-plane effective thermal conductivities of plain-weave fabric composites based on a thermal-electrical analogy. The work showed closed-form solutions of the effective thermal conductivities in the warp and fill directions. In order to affirm the applicability of these solutions, the in-plane effective thermal conductivities of S-glass, E-glass, graphite, and Kevlar-49 plain-weave fabric-reinforced epoxy composites were presented. H. Yu et al. [2,3] developed a detailed three dimensional finite element model to predict the through-thickness thermal conductivity of a textile composite structure consisting of a woven fabric and matrix in which conductive particles are randomly distributed in the matrix in the unit cell already containing the woven fabric, and the effective thermal conductivity of this three-phase system is numerically evaluated. They results of this three-component system presented were compared with a two-component system in which the thermal conductivity of the matrix and particles is homogenised by a finite element approximation under the same thermal conditions. Y. Liu et al. [4] presented 3D finite element (FE) analysis

to investigate the mechanical behaviour of a typical 3D spacer fabric structure under compression in terms of its structural feature and mechanical properties of its components. A spacer fabric consists of two separate outer layers joined together with spacer monofilaments.

M. Siddiqui et al. [5] developed a method to predict the effective thermal conductivity and thermal resistance of woven fabric by using the finite element method (FEM). Repeating of the unit cell of the fabric was developed using the actual parametric value of the fabric by means of a scanning electron microscope (SEM) and then these unit cells were analyzed by applying different boundary conditions. R. Pasupuleti et al. [6] presented a numerical investigation on the moisture diffusion taking place in multilayer woven fabric composites. The transient diffusion process of moisture is examined based on the repeating Representative Unit Cell (RUC) of woven fabrics. Using finite element analysis methods, the microscopic heterogeneity of RUC was described in terms of the tow size, tow cross-section shape and tow weaving configuration of fabrics. The model was then applied to simulate the moisture diffusion within the composites of a varied number of plies. The study of X. Zeng [7] proposes a modelling approach which is based on geometrical data and self-imposed kinematic constraints of interweaving yarns to simulate woven fabric structures under realistic manufacturing conditions. The implementation is automated in the open source software TexGen for generation of geometrical textile models. The commercial code ANSYS/CFX is employed for Computational Fluid Dynamics (CFD) analysis of impregnating flow through the fabric geometries generated as a pre-requisite for fabric permeability determination. The approach is evaluated for two woven fabric lay-ups at controlled compression and/or shear deformation. J. Schuster et al. [8] investigated the effect of three-dimensional fibre reinforcement on the out-of-plane thermal conductivity of composite materials. Composite preforms were 3D orthogonally woven with pitch carbon yarns and plied copper wires in the thickness direction. After infusion using a vacuum-assisted resin transfer moulding process, the out-of-plane thermal conductivities of the resultant composites measured showed a significant increase compared to a typical laminated uniaxially or biaxially reinforced composite. Using finite element models to better understand the behaviour of the composite material, improvements to an existing analytical model were performed to predict the effective thermal conductivity as a function

of the composite material properties and in-contact thermal material properties. The aim of the article is associated with the problem of thermal comfort. Zhu FL. and Zhou Y. in their work presented a theoretical model to predict simultaneous heat and moisture transfer based on Fourer's law and Fick's second law. The dynamic diffusivity characterised by the Luikov and Arrhenius equations is involved in the mass transfer equation. In order to validate the mathematical model proposed, fire testing protection (FTP) measurements were carried out to measure the thermal protective performance of firefighters' protective clothing [9].

Mehrnoosh Rahnama et al. [10] designed an intelligent model of heat and moisture propagation in light nonwoven fabrics by the conversion of a numerical propagation model of a partial differential equation to a feed forward propagation neural network. Propagation coefficients of heat and moisture transfers were estimated from the intelligent model for nonwoven samples containing hydrophilic natural and hydrophobic synthetic fibres.

In the work of Radostina A. Angelova et al. the effect of the convective boundary layer around the human body on the transfer of heat through a single textile layer was showed numerically. A new approach of presenting a numerical model of a textile surface transmitting heat by convection to the surroundings was presented. CFD simulations were used to study the influence of the speed of CBL and its size on the ability of the textile structure to transfer heat in the through-thickness direction of the sample [11].

In this article, studies on the problems of textiles thermal insulation are shovn, comprising a continuation of investigations carried out in the earlier two works [12, 13] The main goal of the first one was to conduct the modelling of heat transfer through 3D weft knitted polypropylene fabric. The novel element of this work was the physical and local description made within SolidWorks software, which had not been previously available for use with reference to textile structures. Additionally the original sensitivity analysis of the temperature field in relation to knitting morphology was conducted and could provide instructive tools for its future application. The subjects of the second work were double-layer knitted fabrics with potential application in multi-layer garments addressed to newborns. The materials studied were constructed from the following raw materials: cotton, polypropylene, polyester, polyamide, bamboo, and viscose. Knitted fabrics with a comparable geometric

structure and different composition were tested for their thermal insulation. In the xperimental section, the temperature changes in specific constant ambient conditions were investigated using a thermal imaging camera. The main goal of this paper was to design an optimal model of textiles by means of SolidWorks software, and to carry out theoretical research on their thermal insulation, where results can be confirmed by tests on actual materials.

The subject of current work were multi-layer textiles with potential application in garments addressed to a specific group of users. The materials studied were constructed with the following raw materials: Kevlar, Nomex, ePTFE/PU bicomponent and carbon fibre. The multi-layer materials, with a comparable geometric structure and similar composition, were tested for their thermal insulation. In the experimental part, the temperature change in specific constant ambient conditions was investigated using a thermal imaging camera. In the simulation part 3-D models of actual textiles were designed and the temperature change calculated on the basis simulations performed . The main goal of this paper was to design an optimal model of textiles to carry out theoretical research of their thermal insulation, whose results can be confirmed by tests on actual materials. In the simulation part, 3-D models of the textiles, constructed by SolidWorks 2014 software, of yarn mapping of varying accuracy were designed and the temperature change calculated on the basis simulations performed.

■ Materials and methods

The subject of the study were 3 multi-layer systems intended for a firefighter's uniform (UTP 6, UTP 7 and UTP 9). All the uniforms are made of three layers:
1) outer fabric,
2) composite layer consisting of a membrane (film) and nonwoven fabric,
3) lining layer consisting of nonwoven fabric and inner fabric.

In *Figure 1* an image of UTP 9 obtained by means of high-resolution X-ray micro tomography (SkyScan 1272 model manufactured by Bruker in USA) is presented.

Parameters of the uniforms are presented in *Table 1*.

The aim of this study was to estimate the thermal insulation of the multilayer
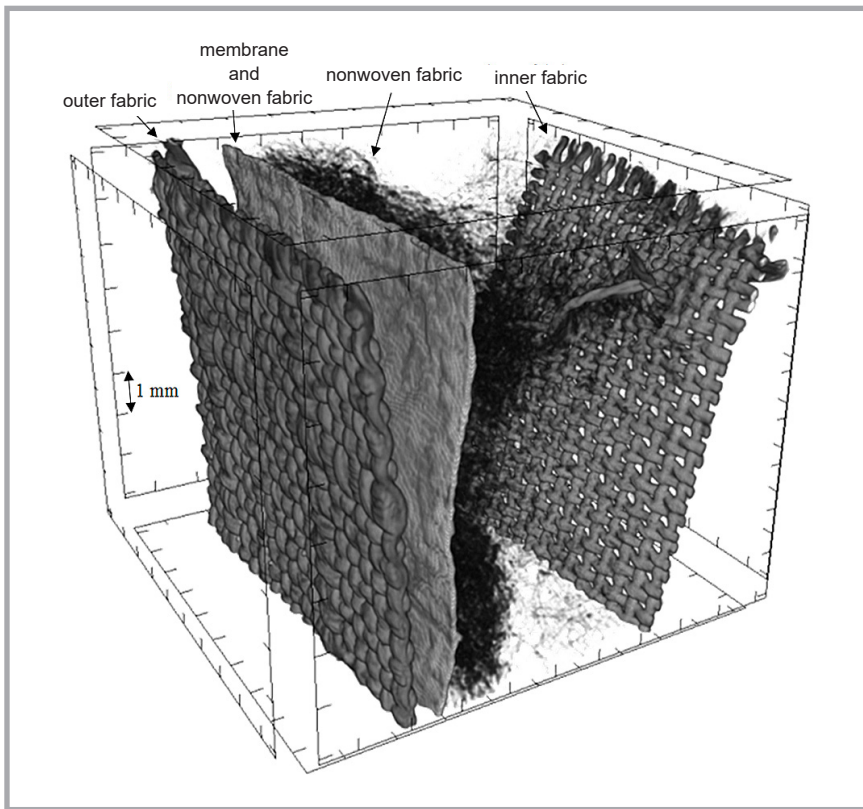
Figure 1. *Image of UTP 9 obtained by means of high-resolution X-ray micro tomography. The layers were intentionally separated in order to improve the readability of the image.*

textiles in conditions comparable to those in a climatic chamber (a so-called model of human skin) during the thermal resistance calculation of the textiles (air temperature, T_{air} – 20 °C, relative humidity, RH– 65%). Studies of the textiles' thermal insulation were divided into two parts – the experimental and simulation.

In the experimental part studies were carried out on the actual materials based on the phenomenon of thermal imaging. In the simulation part, three-dimensional geometric models were created and simulations of heat transport phenomena performed. Both experimental and simu-

lation investigations were conducted in a steady state.

■ Experimental study

To assess the thermal insulation, textiles were placed in a room (Great Climatic Chamber, made by Weiss Technik, Germany) with a constant air temperature (T_{air} = 20 ± 0.1 °C) and constant humidity (RH = 65 ± 1%) on a flat plate (Measurement Technology North West, USA) at a constant temperature (T_{plate} = 35 ± 0.1 °C). In accordance with the construction of the clothing designed, the bottom layer was made of inner fabric (Kevlar or Nomex) and nonwoven fabric (Kevlar), the middle layer - nonwoven fabric (Kevlar) with a membrane (ePTFE/PU Bi component), and the outer layer was of fabric whose main component was Nomex or Kevlar. Using a thermal imaging camera (FLIR SC5000 model, made in the USA) and software included (Altair – Thermal Image Analysis Software), the minimum temperature of the material i.e. temperature of the top surface of the multilayer clothing (facing the environment) was measured. On the basis of the known maximum temperature of the material i.e. the temperature of the bottom surface of the clothing (adjacent to the plate and being in thermal equilibrium with the plate), the temperature change in a direction perpendicular to the surface of the fabric was calculated. The temperature measure-

Table 1. *Characteristics of UTP 6, UTP 7 and UTP 9 obtained according to: EN ISO 5084:1996 [a], EN 12127:2000 [b], EN ISO 2060:1997 [c] and own methodology [d], as described in Experimental study.*

	Layer no.	Layer name	Layer composition	Layer thickness [a], 10^{-3} m	Mass per unit area [b], 10^{-3} kg·m^{-2}	Yarn diameter [c], 10^{-3} m	Fibre diameter [c], 10^{-6} m	Fibre number in yarn [d]	Surface area of yarn in the smallest repetitive element [d], 10^{-3} m^2
UTP 6	1	outer fabric	75% Nomex, 23% Kevlar, 2% carbon fibre	0.42 ± 0.01	210.11 ± 14.71	0.33 ± 0.01	26 ± 0.2	154 ± 5	27.34 ± 2
	2	nonwoven fabric membrane (film)	100% Kevlar 100% ePTFE/PU bicomponent	0.66 ± 0.01 0.06 ± 0.01	155.17 ± 10.86	- -	20 ± 0.2 -	- -	- -
	3	nonwoven fabric's inner fabric	100% Kevlar 100% Kevlar	1.94 ± 0.01 0.41 ± 0.01	290.97 ± 20.37	- 0.20 ± 0.01	29 ± 0.2 18 ± 0.2	- 163 ± 5	- 38.53 ± 2
UTP 7	1	outer fabric	75% Nomex, 23% Kevlar, 2% carbon fibre	0.42 ± 0.01	210.11 ± 14.71	0.33 ± 0.01	27 ± 0.2	161 ± 5	29.34 ± 2
	2	nonwoven fabric membrane (film)	100% Kevlar 100% ePTFE/PU bicomponent	0.48 ± 0.01 0.06 ± 0.01	98.87 ± 6.92	- -	20 ± 0.2 -	- -	- -
	3	nonwoven fabric's inner fabric	100% Kevlar 100% Kevlar	1.94 ± 0.01 0.41 ± 0.01	290.97 ± 20.37	- 0.20 ± 0.01	28 ± 0.2 19 ± 0.2	- 166 ± 5	- 40.74 ± 2
UTP 9	1	outer fabric	78% Nomex, 20% Kevlar, 2% carbon fibre	0.44 ± 0.01	219.53 ± 15.37	0.32 ± 0.01	27 ± 0.2	165 ± 5	29.44 ± 2
	2	nonwoven fabric membrane (film)	100% Kevlar 100% ePTFE/PU bicomponent	1.68 ± 0.01 0.06 ± 0.01	245.38 ± 17.18	- -	20 ± 0.2 -	- -	- -
	3	nonwoven fabric's inner fabric	100% Nomex 100% Nomex	1.85 ± 0.01 0.41 ± 0.01	280.91 ± 19.66	- 0.20 ± 0.01	28 ± 0.2 19 ± 0.2	- 166 ± 5	- 40.74 ± 2

ments were performed for samples with an area of approximately $25 \cdot 10^{-2}$ m², but the real sample size was larger (about $50 \cdot 10^{-2}$ m²) in order to reduce the impact of boundary conditions. Measurements of every material were carried out after reaching a steady state (about 10 minutes). Measurement errors of the temperature resulting from thermal imaging camera specifications was ±1 °C. A scheme of the experiment is presented in *Figure 2*.

■ Simulation study

The main aim of this part of the work was to create a three-dimensional model of tested textiles as a potential components of multi-layer uniforms providing thermal balance between the user and the environment. Two 3-D models of the textiles were made in SolidWorks 2014 software that differ in the degree of accuracy of reproduction fabrics (example in *Figure 3*).

In the first approach, the model developed (so-called *mono-fibre model*) does not take into account individual fibres in the fabrics (the yarn as a single-component, continuous object – monofilament). For each fabric, separate a *mono-fibre model* was created taking into account the following different physical parameters of the textiles:
1) fabric thickness,
2) yarn diameter (equivalent diameter, since the actual yarns did not have a circular cross-section).
In second approach, to better reproduce the fabric's thermal properties, a new model was created (a so-called *multi-fibre model*). This model takes into account the same two physical parameters of the textiles from the *mono-fibre model;*

however, it also maps the internal structure of the yarn, including the fibre shape:
3) fibre diameter and
4) fibre number in yarn.

In both models for each textile, the fabric thickness, layer thickness and yarn diameter were the same (all according to *Table 1*). The average fabric thickness (*Table 1*) was experimentally measured according to Standard EN ISO 5084 1996. The yarn equivalent diameter was estimated based on stereoscopic optical microscope images (fibre diameter was measured based on scanning electron microscope images) using *Image J* software and mapped into the design of the 3-D models. The specific surface area of yarn was calculated on the basis of knowledge of the fibre number. In both models, the circular cross-section of the yarn, as well as the circular cross-section of the fibre in the *multi-fibre model* were assumed.

In both models, nonwoven fabric, due to its complicated chaotic arrangement of fibres, was mapped as rectangular porous media of isotropic porosity, where P was calculated on the basis of the mass per unit area – M_p, thickness – d and density of the raw material – ρ, according to the formula:

$$P = \left(1 - \frac{M_p \cdot 10^{-3}}{d \cdot \rho}\right) \cdot 100\% \qquad (1)$$

Membranes (films) were mapped as rectangular continuous layers. *Figure 4* shows the following steps in designing a *multi-fibre model* of outer fabric (plain weave) in a UTP 6 uniform. Because of the wavy shape and periodic arrangement of the warp and weft, the model was designed based on the following average geometric parameters: wavelength,
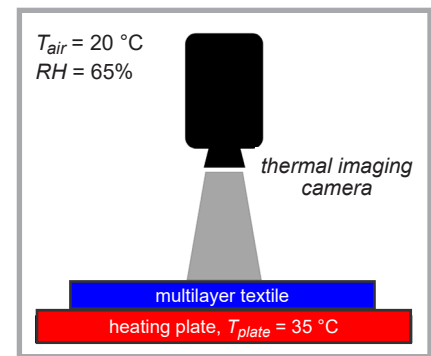
amplitude, yarn diameter, and yarn and fibre length in the smallest repetitive element (repeat), estimated based on stereoscopic optical microscope images using *Image J* software. Additional parameters were the fabric thickness and layer thickness (EN ISO 5084 1996). The first stage in designing the model was to create two-dimensional sketches of the axis of the warp on parallel planes using NURBS-curves (*Figures 4.a, 4.b*). The next steps were to create two-dimensional sketches of the axis of the weft on parallel planes perpendicular to the previous two (*Figures 4.c, 4.d*). The next step of the design was to prepare a cross-sectional sketch of yarn built of individual fibres (*Figure 4.e*). The final shape of the yarn in the warp and weft was obtained using the *swept boss/base* operation performed on the objects that were created in the last three steps (*Figures 4.f – 4.j*). Thus duplicating the objects created, a ready model of the fabric was obtained.
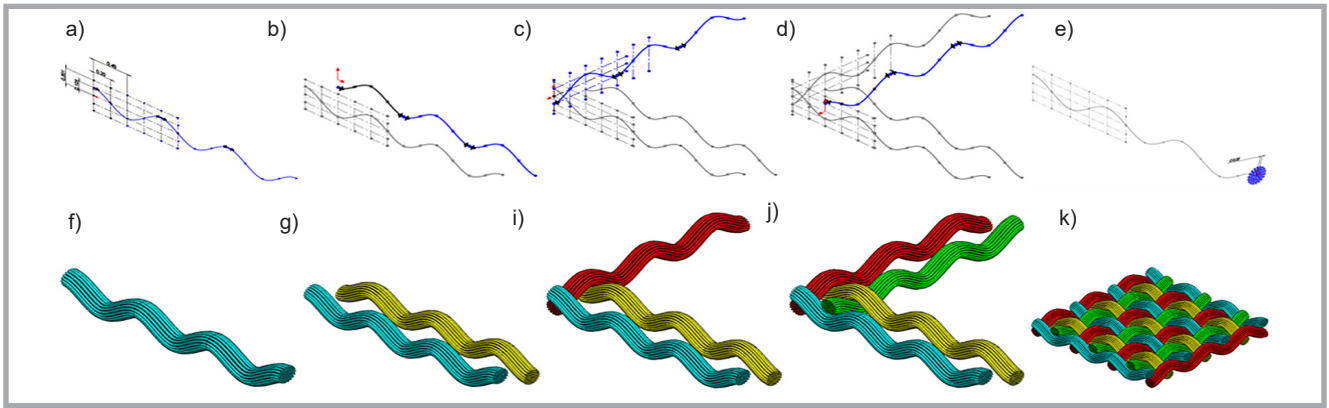
Theoretical basis of modelling

Equations describing the simulation of heat transfer

Flow Simulation solves the Navier-Stokes equations, which are formulations
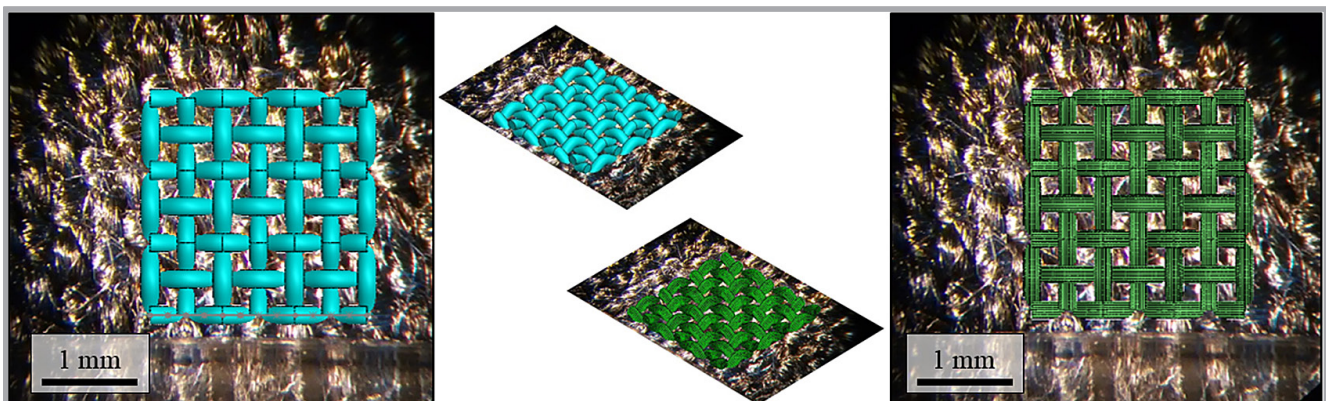
Figure 3. Mono-fibre model (blue) and multi-fibre model (green) of the outer fabric of UPT 6 made on the basis of stereoscopic optical microscope images.

Figure 4. Stages of designing of 3-D multi-fibre model fabric (the diameter of the fibres was intentionally increased in relation to the real sizes (**Table 1**) in order to improve the readability of the scheme).

using mass, momentum and energy conservation laws for fluid flows. The equations are supplemented by fluid state equations defining the nature of the fluid and by empirical dependencies of fluid density, viscosity and thermal conductivity on temperature [14]. The system of Navier-Stokes equations is supplemented by definitions of thermophysical properties and state equations for fluids. Flow Simulation models gas and liquid flows with density, viscosity, thermal conductivity, specific heat, and species diffusivities as functions of pressure, temperature and species concentrations in fluid mixtures. The equilibrium volume condensation of water from steam can also be taken into account when simulating steam flows.

Fabric is a complex structure of fibres and void spaces between fibres filled by fluid, such as air or liquid. Heat is transported through the textile structure through both monofilaments (solid body) and fluids (fluid media), with simultaneous exchange between these environments. Heat transfer in fluids is expressed by the following conservation **Equation 2**, where $S_i = S_i^{porous} + S_i^{gravity} + S_i^{rotation}$ is the volume-distributed external force per unit volume (in N·m^{-3}) due to porous media resistance (S_i^{porous}), buoyancy ($S_i^{gravity}=-\rho g_i$) and coordinate system rotation ($S_i^{rotation}$). The subscripts are used to denote summation of the three coordinate directions.

The heat flux density is defined by the following equation:

$$q_i = \left(\frac{\mu}{Pr} + \frac{\mu_t}{\sigma_c} \right) \frac{\partial h}{\partial x_i}; \quad i = 1, 2, 3; \quad (3)$$

where,

$$\mu_t = \frac{C_\mu \rho k^2}{\zeta} . \quad (4)$$

Constant C_μ is determined according to [14] as equal to $C_\mu = 0.09$, and $\sigma_c = 0.9$. The equations describe both laminar and turbulent flows. Moreover transitions from one case to another and back are possible, where k is turbulent kinetic energy and ζ, J·kg^{-1}·s^{-1} is the turbulence dissipation (rate at which turbulence kinetic energy is converted into thermal internal energy). Parameters k and μ_t are zero for pure laminar flows. The phenomenon of anisotropic heat conductivity in solid media is described by the following correlation:

$$\frac{\partial(\rho e)}{\partial t} = \frac{\partial}{\partial x_i} \left(\lambda_i \frac{\partial T}{\partial x_i} \right) + Q_H; \quad (5)$$

where, $e = cT$. It is assumed that the heat conductivity tensor is diagonal to the coordinate system considered and that the heat transport within polypropylene is direction-independent, i.e., we introduce an isotropic medium and can denote $\lambda_1 = \lambda_2 = \lambda_3 = \lambda$. The energy exchange between the fluid and solid media is calculated via the heat flux in the direction normal to the solid/fluid interface, taking into account the solid surface temperature and fluid boundary layer characteristics, if necessary.

■ Thermal radiation

Flow Simulation enables the simulation of thermal radiation based on a so-called *discrete transfer model*. Its main idea can be described as follows: The radiation leaving the surface element in a certain range of solid angles can be approximated by a single ray. The radiation heat is transferred along a series of rays emanating from the radiative surfaces only. Rays are then traced as they traverse through fluid and transparent solid bodies until they hit another radiative surface. This approach, usually called "ray tracing," allows "exchange factors" to be calculated as fractions of the total radiation energy emitted from one of the radiative surfaces that is intercepted by others (this quantity is a discrete analog of view factors). If the "exchange factors" between radiative surface mesh elements are calculated at the initial stage of the solver, then it allows a matrix of coefficients to form for a system of linear equations which can be solved at each iteration. The surfaces that lose heat by radiation can emit, absorb and reflect solar or thermal radiation. The thermal radiation determined by the surface or radiation source is expressed as a sum of material radiation (described by the surface emissivity and prescribed area of radiation) and incoming radiative transfer. This problem is defined by the **Equation 6** [14]:

$$Q_T^{out} = \varepsilon \cdot \sigma \cdot T^4 \cdot A + (1 - \varepsilon) \cdot Q_T^{in} . \quad (6)$$

$$\frac{\partial}{\partial t}\left[\rho\left(h + \frac{u^2}{2} \right) \right] + \frac{\partial}{\partial x_i}\left[\rho u_i \left(h + \frac{u^2}{2} \right) \right] = \frac{\partial}{\partial x_i}\left[u_j\left(\tau_j + \tau_j^R \right) + q_i \right] + \frac{\partial p}{\partial t} - \tau_{ij}^R \frac{\partial u_i}{\partial x_j} + \rho\varepsilon + S_i u_i + Q_H \qquad (2)$$

Equation 2.

The main result of the radiation heat transfer calculation is the solid's surface or internal temperature. However, these temperatures are also affected by heat conduction in solids and solid/fluid heat transfer. To see the results of radiation heat transfer calculation only, the user can view the *leaving radiant flux* over selected radiative surfaces at surface plots. Users can also see the maximum, minimum, and average values of these parameters.

■ Heat flow in porous media

Porous media are treated in flow simulation as distributed resistances to fluid flow, hence they cannot occupy the whole fluid region or fill the dead-end holes. In addition, if the heat conduction in solids option is switched on, the heat transfer between the porous solid matrix and t fluid flowing through it is also considered. Therefore the porous matrix acts on the fluid flowing through it via the Si, Siui, and (if heat conduction in solids is considered) Q_H terms in *Equation 2*, whose components related to porosity are defined as:

$$S_i^{porous} = -k \cdot \delta_j \cdot \rho \cdot u_j \qquad (7)$$
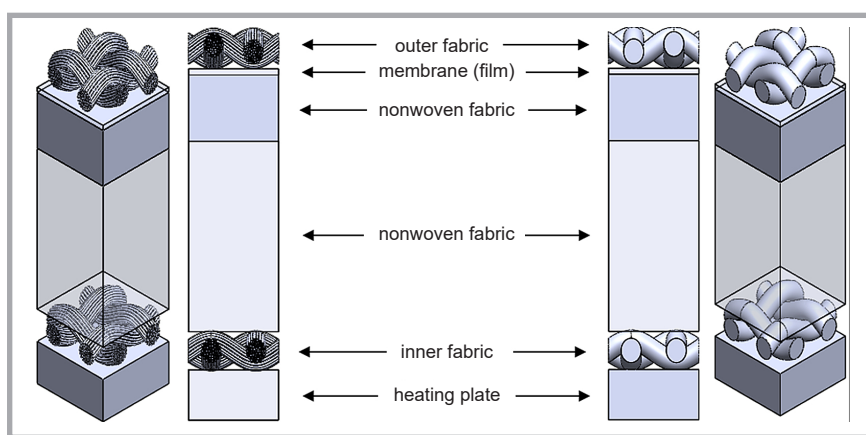
$$Q_H^{porosity} = \gamma \cdot (T_p - T) \qquad (8)$$

where, k is the resistance vector of the porous medium, γ the user-defined volumetric porous matrix/fluid heat transfer coefficient, T_p the temperature of the porous matrix, and T is the temperature of the fluid flowing through the matrix. In addition, the fluid density in *Equation 2* is multiplied by the porosity n of the porous medium, which is the volume fraction of the interconnected pores with respect to the total medium volume.

The thermal conductivity of the porous matrix can be specified as anisotropic in the same manner as for the solid material. The conjugate heat transfer problem in a porous medium is solved under the following restrictions:
■ heat conduction in a porous medium not filled with a fluid is not considered,
■ porous media are considered transparent for radiation heat transfer,
■ heat sources in the porous matrix can be specified in the forms of the heat generation rate or volumetric heat generation rate only; heat sources in the form of a constant or time-dependent temperature cannot be specified.

To perform a calculation in flow simulation, it is necessary to specify the following porous medium properties: the effective porosity of the porous medium, defined as the volume fraction of interconnected pores with respect to the total medium volume. Later on, the permeability type of the porous medium must be chosen from among the following:
■ isotropic (i.e., the medium permeability is independent of the direction),
■ unidirectional (i.e., the medium is permeable in one direction only),
■ axisymmetrical (i.e., the medium permeability is fully governed by its axial and transversal components with respect to a specified direction),
■ orthotropic (i.e., the general case, when the medium permeability varies with the direction and is fully governed by its three components determined along the three principal directions).
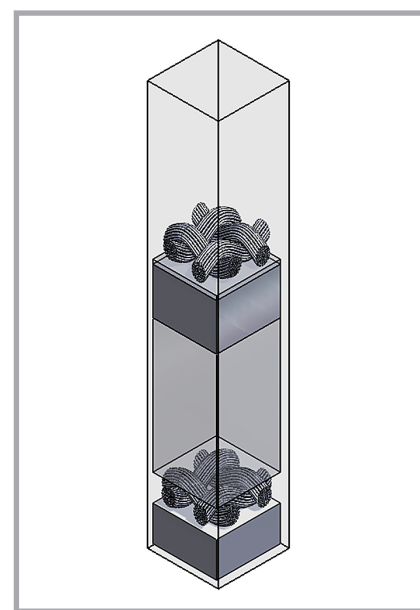
Simulations of thermal insulation

Simulations were determined with the SolidWorks Flow Simulation module using the finite volume method. For the purposes of the simulation all models of the textiles were reduced to the smallest repetitive element with a surface area of about 10^{-3} m^2. In *Figure 5* the *mono-fibre-model* and *multi-fibre-model* for material UPT 6 are presented.

The multilayer textile models were situated on the top surface of a rectangular plate that served as a heater. Both elements were positioned on the bottom of a rectangular computational domain, with a volume equal to $4.8 \cdot 10^{-9}$ m^3 $(5.0 \times 1.0 \times 1.0) \cdot 10^{-3}$ m, which was filled with air (*Figure 6*).

To eliminate the effects of asymmetric boundary conditions, settings were applied to imitate an infinite layer of fabric propagating outside of the domain in all three directions. The initial conditions of the model were assumed as follows: $T_{plate} = 35$ °C, $T_{textile} = 20$ °C,

$T_{air} = 20$ °C, $p_{air} = 1013.25$ hPa and $RH = 65$ %. The computational domain was divided into approximately 570 000 cells of three types (fluid cells, solid cells and partial cells). Fluid cells were filled with air, while solid cells had the material characteristics of the uniform, the heating plate or both the uniform and heating plate. The partial cells contained both solid material and air. The number of cells was dependent on the number and size of the elements making up the model of a particular multilayer system. A much larger number of cells in the *multi-fibre* model in comparison to the *mono-fibre* model resulted from the

Figure 5. *Mono-fibre model (right) and multi-fibre model (left) of UPT 6 textile positioned on the heating plate (in the multi-fibre model the diameter of the fibres was intentionally increased in relation to the real sizes (Table 1) in order to improve the readability of the scheme).*

Labels: outer fabric, membrane (film), nonwoven fabric, nonwoven fabric, inner fabric, heating plate

Figure 6. *Multi-fibre model of UTP 6 positioned on a heating plate located on the bottom of a computational domain of size $(5.0 \times 1.0 \times 1.0) \cdot 10^{-3}$ m (diameter of the fibres was intentionally increased in relation to the real sizes (Table 1) in order to improve the readability of the scheme).*

Table 2. *Physical parameters applied in simulations.*

Physical parameter	Nomex	Kevlar	PTFE	PU
Density, kg·m⁻³	1380	1440	2200	1200
Specific heat, J·kg⁻¹·°C⁻¹	1396	1200	1300	1120
Thermal conductivity, W·m⁻¹·°C⁻¹	0.09	0.04	0.25	0.035
Emissivity (for black body = 1)	0.65	0.50	0.85	0.90
Porosity of nonwoven fabric in layer 2, %	70			
Porosity of nonwoven fabric in layer 3, %	90			
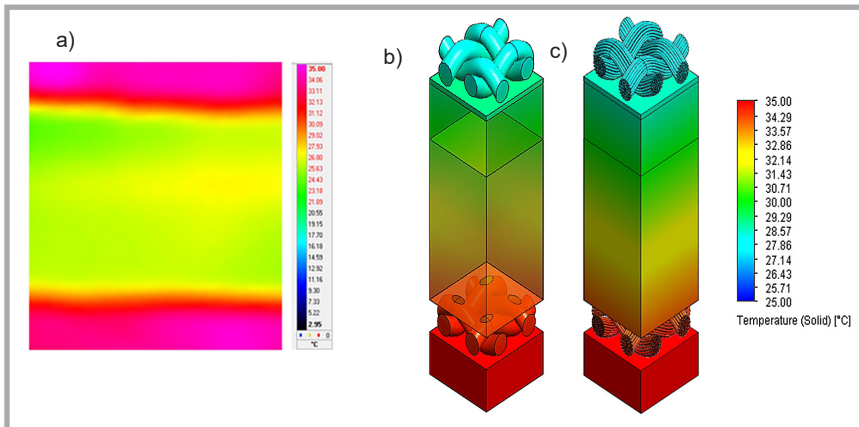
Figure 7. *Sample thermal image obtained by measurement of the temperature distribution on the top surface of UTP 6 (a) and temperature distribution on the surface of 3-D models of UTP 6 obtained from simulations for mono-fibre model (b) and multi-fibre model (c); (in multi-fibre model the diameter of fibres was intentionally increased in relation to the real sizes (**Table 1**) in order to improve the readability of pictures); different palettes of colour and ranges of temperatures were applied as a result of different software applications (Altair – Thermal Image Analysis Software and SolidWorks Flow Simulations).*

mapping of individual fibres. In the *multi-fibre* model the largest number of cells were partial ones (approximately 48%), followed by fluid cells (about 44%) and solid cells (about 8%). The *Mono-fibre* model consisted of partial cells (approximately 45%), fluid cells (about 43%) and solid cells (about 12%). The number of cells was selected optimally so that

the larger number of elements did not result in significant differences in the results calculated.

In **Table 2**, physical parameters of raw materials applied in the 3-D geometric models of the textiles were presented. Emissivity was obtained experimentally according to the following procedure:

Before starting the investigations, the results of which are presented in the article, the following calibration of the infrared camera was performed to select the right emissivity for each raw material (Nomex, Kevlar, PTFE):

1) Layers were separated from each other and placed in an air conditioned chamber with a constant temperature of 20 °C and *RH* = 65%.

2) After 24 hours (when the materials and air were in thermal equilibrium) temperature measurements for each raw material were performed (emissivity of the raw material was chosen so that the camera indicated the real temperature of the layer: 20 °C).

The two steps above were repeated for temperatures of 30 °C and 40 °C (always for *RH* = 65%). The three other parameters: specific heat, thermal conductivity and density of all raw materials were taken from the following literature [15, 16].

■ Results and comments

The SolidWorks Flow Simulation module allows to mode the following five physical phenomena:
1) heat conduction in a solid material (i.e., fibres of the fabric structure),
2) convection and
3) radiation heat transfer from solid surfaces,
4) gravitational effects influencing air molecule transport within void spaces, and
5) laminar and turbulent fluid flow within void spaces.

The software simultaneously calculates the parameters of all selected thermo-
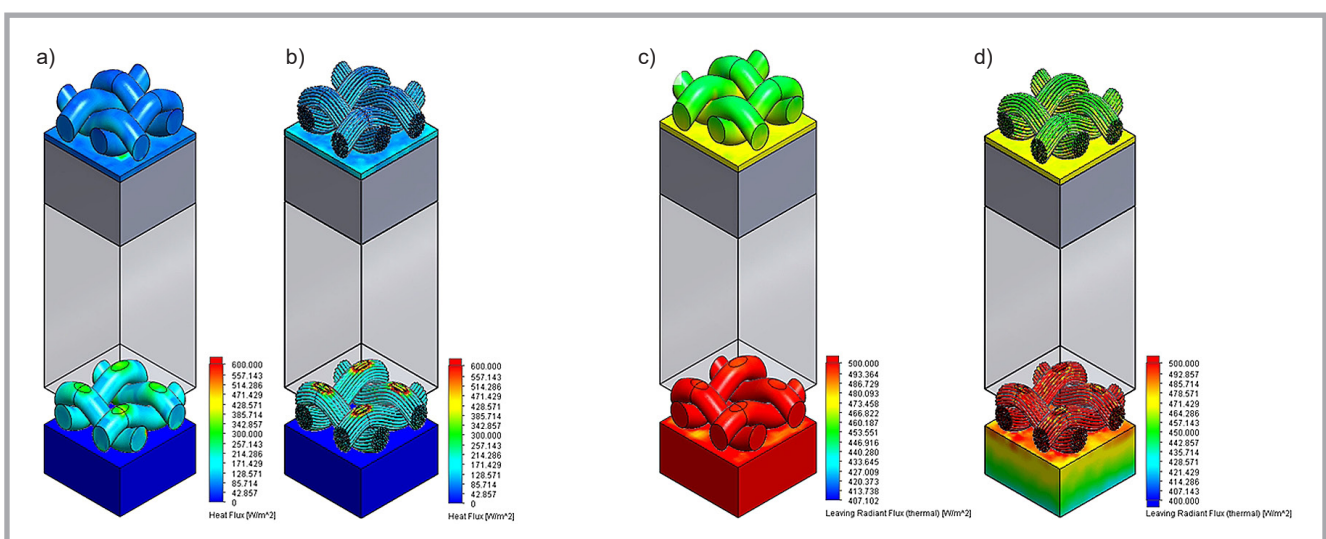
Figure 8. *Sample of distributions of heat flux (a – mono-fibre model, b – multi-fibre model) and leaving radiant flux (c – mono-fibre model, d – multi-fibre model) in UTP 6 (in multi-fibre model the diameter of the fibres was intentionally increased in relation to the real sizes (**Table 1**) in order to improve the readability of pictures).*

dynamic processes within the structural computational domain assumed. Based on the output results, the software creates three-dimensional colour visualizations on the surfaces of the entire model or its selected parts. For the models of textiles previously mentioned, the distribution of temperature (*Figures 7.b* and *7.c*), heat conductivity (*Figures 8.a* and *8.b*) and heat radiation, as the most effective method of heat loss (*Figures 8.c* and *8.d*), were determined. The software does not allow to specify nor illustrate of energy losses by convection only, despite the fact that this phenomenon is taken into account. In *Figure 7.a*, sample thermal images obtained during measurement of the temperature distribution of both the top surface of UTP 6 and on the surface of the simulated 3-D models are presented.

As a result of the simulations, the following parameters of the multilayer textiles were also calculated (*Table 1*):

- the minimum temperature of the material, i.e., the temperature on the top surface of the outer fabric, which faces the environment;
  The maximum temperature of the multilayer uniform, i.e., the temperature on the bottom surface of the inner fabric, which is adjacent to and in thermal equilibrium with the plate, was assumed to be equal to 35 °C, and was not calculated (calculating error equal to 0).
- the average heat flux (*HF*, W·m⁻²) on the surface of the top and bottom layer of the multilayer uniform; and
- the average leaving radiant flux (*LRF*, W·m⁻²) on the surface of the top and bottom layer of the multilayer uniform.

Heat flux and leaving radiant flux results are presented in the graph in *Figure 9*. Both in *Table 3* and *Figure 9*, calculation errors were present (Δ*T*, Δ*HF*, Δ*LRF*), resulting from the geometry of the model and the finite volume mesh density.

Simulations carried out on the *mono-fibre model* and *multi-fibre model* for the heat flux and leaving radiant flux showed comparable results. Accordingly all three
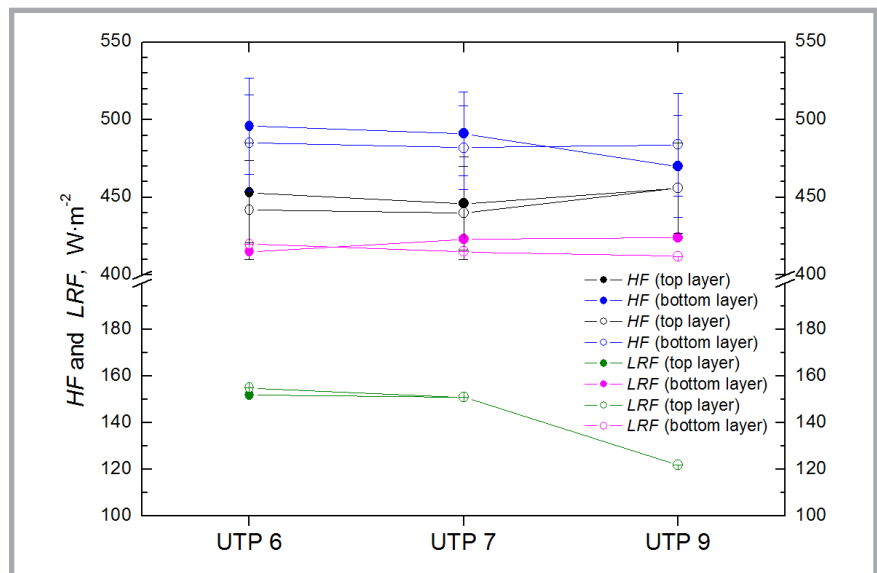

Figure 9. Simulation results of heat flux and leaving radiant flux for the top and bottom layer of the textiles (full symbols indicate the mono-fibre model, empty symbols - the multi-fibre model); broken curves guide the eye.

multilayer materials lost a lot of energy through the bottom layer (the highest temperature) as a result of the thermal conductivity (heat flux in the range of 470 – 496 W·m⁻²) and by thermal radiation (leaving radiant flux in the range of 415 – 424 W·m⁻²) for the *mono-fibre model,* while for the *multi-fibre model* the heat flux was in the range of 482 – 485 and the leaving radiant flux - in the range of 412 – 421 W·m⁻². Because of the lower temperature of the upper layer, the heat loss from it is smaller, which is particularly evident in the case of losses by radiation (which is characterised by a stronger temperature dependence than the thermal conductivity). For the *mono-fibre model,* the leaving radiant flux was in the range of 122 – 151 W·m⁻², while for the *multi-fibre model* the leaving radiant flux was in the range of 121 – 155 W·m⁻². As expected, the lowest value of *LRF* was achieved for UTP 9 (highest thickness), where the temperature of the top layer had the lowest value. In the case of losses by thermal conductivity, the heat flux was in the range of 446 – 456 W·m⁻² for the *mono-fibre model* and 442 – 455 W·m⁻² for the *multi-fibre model*. Differences in these models obtained probably result from of the inclusion of

air between individual fibres in the fabric in the *multi-fibre model*. The quantity of the air is different for each fabric because of differences in the fibre diameter. The size of individual fibres affects the surface area through which heat transfer takes place as a result of both conduction and radiation.

The outcomes obtained from measurements using a thermal imaging camera showed a correlation between the uniform thermal insulation, the raw materials from which they were made and their thickness. The highest thermal insulation was shown by the thickest uniform. The largest temperature change – Δ*T* was observed for the UTP 9 uniform, characterised by the highest thickness (1.68×10⁻³ m) of Kevlar nonwoven fabric in layer 2 – 9.82 °C. For the other two uniforms, smaller and comparable values were obtained (UTP 6 – 8.73, UTP 7 – 8.70).

A comparison of experimental and simulation data is presented in *Table 4* and *Figure 10.*

Table 3. Physical parameters calculated in simulations.

No	top layer bottom layer	Experiment		Mono-fibre model						Multi-fibre model					
		T, °C	ΔT, °C	T, °C	ΔT, °C	HF, W·m⁻²	ΔHF, W·m⁻²	LRF, W·m⁻²	ΔLRF, W·m⁻²	T, °C	ΔT, °C	HF, W·m⁻²	ΔHF, W·m⁻²	LRF, W·m⁻²	ΔLRF, W·m⁻²
UPT 6	outer fabric	26.27	1	27.52	0.01	453	32	152.13	0.04	26.99	0.014	442.78	32	155.47	0.04
	inner fabric	35.00	0	35.00	0	496	31	415.26	0.03	35.00	0	485.49	31	420.64	0.02
UPT 7	outer fabric	26.30	1	27.24	0.01	446	30	151.47	0.04	27.02	0.015	440.07	30	151.67	0.03
	inner fabric	35.00	0	35.00	0	491	27	423.91	0.02	35.00	0	482.96	27	415.93	0.04
UPT 9	outer fabric	25.18	1	26.48	0.02	456	29	122.02	0.03	26.03	0.016	455.74	29	121.41	0.02
	inner fabric	35.00	0	35.00	0	470	33	424.49	0.04	35.00	0	484.66	33	412.13	0.03

Table 4. *Experimental and simulation results for temperature change in the multilayer uniforms studied.*

Uniform	ΔT , °C		
	Experiment	**Mono-fibre model**	**Multi-fibre model**
UTP 6	8.73 ± 1	7.48 ± 0.02	8.01 ± 0.02
UTP 7	8.70 ± 1	7.76 ± 0.02	7.98 ± 0.02
UTP 9	9.82 ± 1	8.52 ± 0.01	8.97 ± 0.02
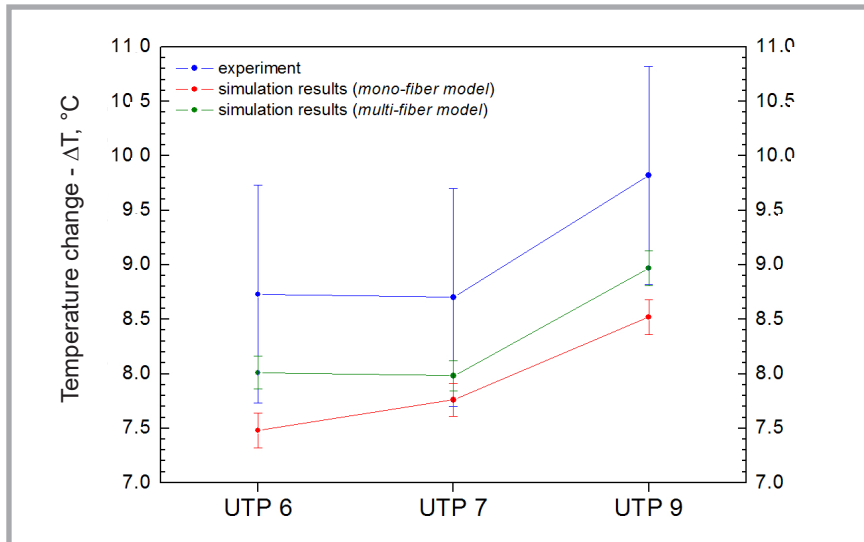
Figure 10. *Experimental and calculated values of temparature change for the multilayer uniforms studied.*

The simulation results showed a similar relationship between the ΔT and the uniform composition and thickness. In the *mono-fibre model,* lower values were obtained (average difference – 1.16 °C) than in the experimental results for all of the materials. The application of the *multi-fibre model* resulted in better compliance with experimental results (average difference – 0.76 °C), and differences were within the range of measurement error of the thermal imaging camera (i.e., less than 1 °C). In the near future, the *multi-fibre model* will be further developed to improve the effective method of designing textiles with desired thermal insulation properties.

◼ Conclusions

In the work, studies on the textile thermal insulation problem were conducted. The subject of the investigations were three multi-layer systems of comparable geometric structure and similar composition constructed with Kevlar, Nomex, ePTFE, PU and carbon fibre. The thermal insulation was tested by experiment using a thermal imaging camera and by simulations of heat transfer phenomena in 3-D models of real textiles. The main aim of the work was experimental verification of two models of a different degree of mapping the morphology of the yarn in the fabrics. The results obtained lead to the following conclusions:

◼ results obtained by simulation for both 3-D models of multilayer systems correlate with experimental results,

◼ values of the temperature difference, ΔT, obtained using the *multi-fibre model* are closer to the results when using a thermal imaging camera,

◼ both experimental and simulation data showed a strong relationship between thermal insulation and physical characteristics (composition and geometric structure),

◼ simulation outcomes showed that the software applied can be an effective tool to complement experimentation on real materials and can be used to predict the thermal properties of newly designed textiles.

References

1. Qiong-Gong N, Tsu-Wei C. Closed-form solutions of the in-plane effective thermal conductivities of woven-fabric composites. *Composites Science and Technology* 1995; 55: 41–48.

2. Yu H, Heider D and Advani S. Prediction of effective through-thickness thermal conductivity of woven fabric reinforced composites with embedded particles. *Composite Structures* 2015; 127: 132–40.

3. Yu H, Heider D, Advani S. Comparison of two finite element homogenization prediction approaches for through thickness thermal conductivity of particle embedded textile composite. *Composite Structures* 2015; 133: 719–726.

4. Liu Y and Hu H. Finite element analysis of compression behavior of 3D spacer fabric structure. *International Journal of Mechanical Sciences* 2015; 94-95: 244–259.

5. Siddiqui M and Sun D. Finite element analysis of thermal conductivity and thermal resistance behaviour of woven fabric. *Computational Materials Science* 2013; 75: 45–51.

6. Pasupuleti R, Wang Y, Shabalin I, Li LY, Liu Z and Grove S. Modelling of moisture diffusion in multilayer woven fabric composites. *Computational Materials Science* 2011; 50: 1675–1680.

7. Zeng X, Endruweit A, Brown L P and Long A C. Numerical prediction of in-plane permeability for multilayer woven fabrics with manufacture-induced deformation. *Composites: Part A* 2015; 77: 266–274.

8. Schuster J, Heider D, Sharp K and Glowania M. Thermal conductivities of three-dimensionally woven fabric composites. *Composites Science and Technology* 2008; 68: 2085–2091.

9. Zhu FL and Zhou Y. Modelling heat-moisture transport through firefighters' protective fabrics from an impinging flame jet by simulating the drying process. *Fibres and Textiles in Eastern Europe* 2013; 21, 5(101): 85–90.

10. Rahnama M, Semnani D and Zarrebini M. Measurement of the moisture and heat transfer rate in light-weight nonwoven fabrics using an intelligent model. *Fibres and Textiles in Eastern Europe* 2013; 21, 6(102): 89–94.

11. Angelova R A, de Bujanda Carasusán A M, Stankov P and Kyosov M. Numerical study of the effect of a natural convective boundary layer around the human body on the transfer of heat through a textile structure. *Fibres and Textiles in Eastern Europe* 2015; 23, 6(114): 131–137. DOI: 10.5604/12303666.1167431.

12. Puszkarz AK, Korycki R and Krucinska I. Simulations of heat transport phenomena in a three-dimensional model of knitted fabric. *AUTEX Research Journal*, DOI: 10.1515/aut-2015-0042 © AUTEX.

13. Puszkarz AK and Krucinska I. The study of knitted fabric thermal insulation using thermography and finite volume method. *Textile Research Journal* DOI: 10.1177/0040517516635999 (2016).

14. SolidWorks Flow Simulation - *Technical Reference,* 2014.

15. Urbańczyk GW. *Fizyka włókna,* Politechnika Łódzka, 2002

16. Włodarski G. *Włókna chemiczne,* WNT, Warszawa.